Three-Carrier Spin Blockade and Coupling in Bilayer Graphene Double Quantum Dots

Chuyao Tong,[1,*] Florian Ginzel,[2] Annika Kurzmann,[1,3] Rebekka Garreis,[1] Lara Ostertag,[1] Jonas D. Gerber,[1] Wei Wister Huang,[1] Kenji Watanabe,[4] Takashi Taniguchi,[5] Guido Burkard,[2] Jeroen Danon,[6] Thomas Ihn,[1] and Klaus Ensslin[1]

[1]*Solid State Physics Laboratory, ETH Zurich, CH-8093 Zurich, Switzerland*
[2]*Department of Physics, University of Konstanz, D-78457 Konstanz, Germany*
[3]*2nd Institute of Physics, RWTH Aachen University, Aachen 52074, Germany*
[4]*Research Center for Functional Materials, National Institute for Materials Science, 1-1 Namiki, Tsukuba 305-0044, Japan*
[5]*International Center for Materials Nanoarchitectonics, National Institute for Materials Science, 1-1 Namiki, Tsukuba 305-0044, Japan*
[6]*Center for Quantum Spintronics, Department of Physics, Norwegian University of Science and Technology, NO-7491 Trondheim, Norway*

(Received 9 November 2022; revised 8 April 2024; accepted 19 May 2024; published 2 July 2024)

The spin degrees of freedom is crucial for the understanding of any condensed matter system. Knowledge of spin-mixing mechanisms is not only essential for successful control and manipulation of spin qubits, but also uncovers fundamental properties of investigated devices and material. For electrostatically defined bilayer graphene quantum dots, in which recent studies report spin-relaxation times T_1 up to 50 ms with strong magnetic field dependence, we study spin-blockade phenomena at charge configuration $(1,2) \leftrightarrow (0,3)$. We examine the dependence of the spin-blockade leakage current on interdot tunnel coupling and on the magnitude and orientation of externally applied magnetic field. In out-of-plane magnetic field, the observed zero-field current peak could arise from finite-temperature cotunneling with the leads; though involvement of additional spin- and valley-mixing mechanisms are necessary for explaining the persistent sharp side peaks observed. In in-plane magnetic field, we observe a zero-field current dip, attributed to the competition between the spin Zeeman effect and the Kane-Mele spin-orbit interaction. Details of the line shape of this current dip, however, suggest additional underlying mechanisms are at play.

DOI: 10.1103/PhysRevLett.133.017001

Spin-orbit and hyperfine interactions are common sources of spin decoherence. Natural bilayer graphene (BLG) is comprised of 98.9% low-mass, nuclear-spin free ^{12}C, and only a small zero-field spin-orbit gap $\Delta_{SO} \approx$ 60–80 μeV has been experimentally observed [1–3]. Investigations of electrostatically defined BLG quantum dots have made great progress recently demonstrating high controlability [1,2,4–11,13]—BLG is now a promising contender as a spin-qubit platform. Recent studies [11,13] reported spin-relaxation times T_1 in BLG quantum dots up to 50 ms, strongly dependent on magnetic field. Understanding the exact spin-mixing mechanisms limiting the lifetimes is thus crucial to successful qubit manipulation and control.

To study spin-mixing mechanisms, it is common to examine the dependence of strength of Pauli blockade on external magnetic fields [14–24], where "standard" double-dot two-carrier charge states (1,1) and (0,2) are investigated [(N_L, N_R) label numbers of carriers in the left and the right dot]. In BLG quantum dots, the valley degree of freedom enriches the energy spectrum [7,9,10,25,26]. Around zero magnetic fields, the two-electron Pauli blockade in BLG is only *valley* in nature [10]—we are thus compelled to move to alternative charge configurations to examine *spin-mixing* effects.

Hence we populate our BLG double dots with three electrons, near the $(1,2) \leftrightarrow (0,3)$ charge transition. By close examination of the states involved, we conclude that around zero magnetic fields the $(1,2) \rightarrow (0,3)$ blockade is *spin* in nature. At various interdot tunnel couplings we study the magnetic field dependencies of leakage currents: In out-of-plane field, we observe a peak in leakage current around zero field, orders of magnitude too wide [19,21,22] to stem from the commonly observed hyperfine-induced spin-mixing effects [14–20], and could instead arise from finite-temperature cotunneling with the leads [24,27,28]. Persistent sharp side peaks, however, point to other spin- and valley-mixing mechanisms at play. In finite in-plane field, we observe leakage current that dips at zero field. This may arise from the competition between the Kane-Mele spin-orbit interaction polarizing the spins of the blocked states fully out of plane [1–3], and the magnetic field that aligns the spin quantization axis in plane, mixing blocked and unblocked states [23]. Compared to similar studies in InAs [15,16], carbon nanotubes [19], and Si [18,24] however, the width of the dips are not strongly

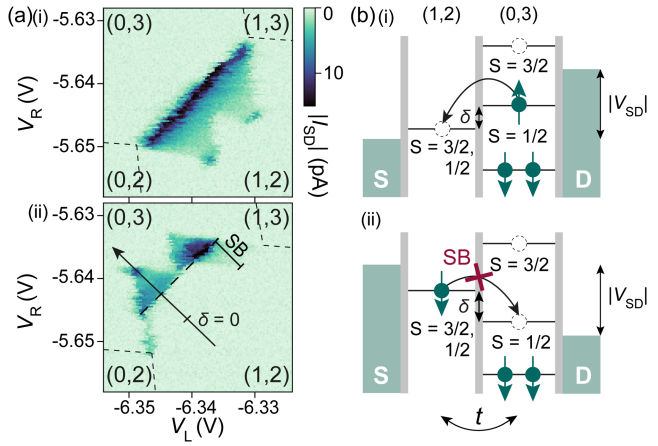

FIG. 1. (a) Bias triangles at zero magnetic-field, at (1,2)–(0,3) charge degeneracy at $V_{MB} = -6.33$ V, (i) $V_{SD} = 1$ mV, $(0,3) \rightarrow (1,2)$, and (ii) $V_{SD} = -1$ mV, $(1,2) \rightarrow (0,3)$. Detuning δ marks the difference between (1,2) and (0,3) ground state electrochemical potential. In (ii) we see regions of strong current suppression by spin blockade. (b) $(1,2) \leftrightarrow (0,3)$ charge transport: (i) any (0,3) state can be split into corresponding (1,2) states, but (ii) transitions from spin-polarized $S_z = \pm 3/2$ (1,2) states to (0,3) is spin blocked.

dependent on interdot coupling, and the magnetic field dependence could be higher order, better described by B^4, than the typical Lorentzian B^2.

Our double quantum dots are defined electrostatically in the same BLG device as described in Ref. [10]. Plunger-gate voltages for the left and the right dot are V_L and V_R, respectively. The interdot t, and dot-lead tunnel couplings, are individually controlled by barrier-gate voltages. For details on the sample structure and quantum dot formation, see Appendix A1 in the Supplemental Material [29].

Finite-bias transport measurements at zero magnetic field close to the (1,2)–(0,3) charge degeneracy are shown in Fig. 1(a), for (i) the $(0,3) \rightarrow (1,2)$ transition, and (ii) the $(1,2) \rightarrow (0,3)$ transition. Strong suppression of current in the lower part of the bias triangles in (ii) signifies the Pauli blockade. To understand its nature, we discuss the relevant single-dot states:

One particle.—Shown in Refs. [1,2], the fourfold degenerate (twofold in spin, $\uparrow$ or $\downarrow$, and twofold in valley, K^- or K^+) ground states are split by the Kane-Mele [3] spin-orbit gap Δ_{SO} into two Kramers pairs: $|\downarrow K^-\rangle$ and $|\uparrow K^+\rangle$ lower in energy, and $|\downarrow K^+\rangle$ and $|\uparrow K^-\rangle$ higher in energy.

Two particles.—The ground state is the threefold degenerate spin-triplet valley-singlet, $|T_s^{\pm(0)} S_v\rangle$ (total spin number $S = 1$, where $S_z = -1$, 0, 1 states are denoted $T_s^{-,0,+}$), due to strong confinements and on-site exchange interaction [7,9,10,25,26].

Three particles.—These are simply the four different states that can result from removing one particle with arbitrary spin and valley, from a fully (fourfold) occupied orbital ground state. The resulting spectrum comprises the four spin-doublet ($S = 1/2$) valley-doublet states, forming Kramers pairs split by Δ_{SO} with $|\downarrow K^-; \uparrow K^+; \downarrow K^+\rangle$ and $|\downarrow K^-; \uparrow K^+; \uparrow K^-\rangle$ lower in energy, and $|\downarrow K^+; \uparrow K^-; \downarrow K^-\rangle$ and $|\downarrow K^+; \uparrow K^-; \uparrow K^+\rangle$ higher in energy. These are the four allowed (0,3) states shown in Fig. S2 [29].

We can now investigate the nature of the blockade resulting from the $(1,2) \rightarrow (0,3)$ transition. The (1,2) charge states have one carrier in the left dot in any of the four single-particle states, and two carriers in the right dot in any of the three spin-triplet valley-singlet states, forming twelve possible (1,2) states in total. At zero magnetic field, these states are split by Δ_{SO}, and can be decomposed into four $S = 1/2$ spin-doublet states with finite tunneling amplitude to the (0,3) $S = 1/2$ spin doublets, and eight blocked $S = 3/2$ spin-quadruplet states [38–40], listed in detail in Appendix A2 [29]. The spin–orbit interaction Δ_{SO} mixes the four spin-quadruplet states with $S_z = \pm 1/2$ with the spin-doublet states (also with $S_z = \pm 1/2$), giving them a finite tunneling amplitude to the (0,3) states.

We are thus left with four *truly* blocked (1,2) states with $S_z = \pm 3/2$, which are product states of the relevant one- and two-particle states in the left and the right dot: $|\uparrow K^{\pm}\rangle_L |T_s^+ S_v\rangle_R$ and $|\downarrow K^{\pm}\rangle_L |T_s^- S_v\rangle_R$. Hence, these states are responsible for the $(1,2) \rightarrow (0,3)$ blockade observed in Fig. 1, which is therefore purely *spin* in nature. At large enough detuning, the excited $S_z = \pm 3/2$ (0,3) states become accessible and lift the blockade, shown by the finite current reappearing at the tip of the triangles in Fig. 1(aii).

To describe the effect of magnetic field on the aforementioned (1,2) states, we employ the Hamiltonian,

$$\hat{H} = \sum_{i=\mathrm{L,R}} \left(g_s \mu_B \mathbf{B} \cdot \hat{\mathbf{S}}_i + g_{v,i} \mu_B B_z \hat{T}_i^z - 2\Delta_{SO} \hat{S}_i^z \hat{T}_i^z \right), \qquad (1)$$

where $\hat{\mathbf{S}}_i = \frac{1}{2}\hat{\boldsymbol{\sigma}}^{(i)}$ is the total spin operator of carriers on dot i and analogously, $\hat{\mathbf{T}}_i = \frac{1}{2}\hat{\boldsymbol{\tau}}^{(i)}$ the total valley pseudospin operator written in terms of the Pauli matrices $\hat{\boldsymbol{\tau}}$ that act in valley space. The first term in (1) describes the usual Zeeman splitting of the spin states, where the electronic g factor $g_s = 2$ [1,2,4,6,7]. The second term adds the coupling of the orbital structure of the valley states to the out-of-plane component of the magnetic field; the corresponding valley g factor is displacement field and dot-geometry dependent [5], measured $g_v \approx 30$ in this device at similar gate configurations [10]. The last term describes the Kane-Mele spin-orbit splitting $\Delta_{SO} \approx 60$–80 μeV between states with their z projection of spin and valley aligned parallel or antiparallel [1–3].

The level structure of the (1,2) states resulting from (1) is sketched in Fig. 2. At zero field, the Kramers pairs on the left dot are split by Δ_{SO}. A finite in-plane field B_x (left) does not couple to the valley degree of freedom, but aligns the spin triplets in the right dot along the x axis and splits them

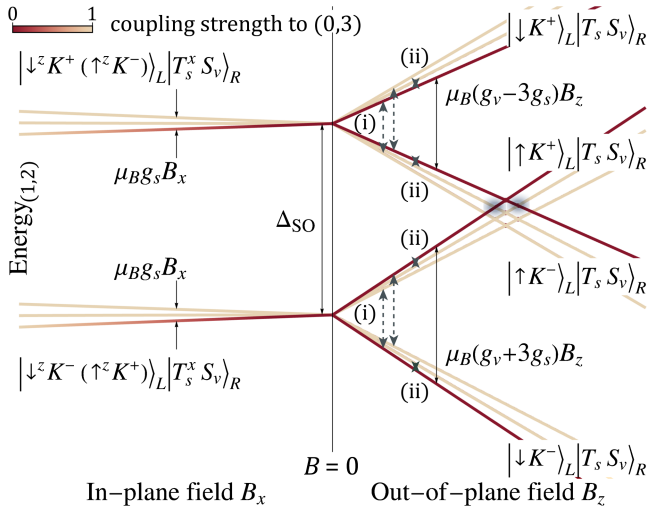

FIG. 2. Level structure of (1,2) states as a function of magnetic fields, resulting from the model Hamiltonian (1). The dark red states ($S_z = \pm 3/2$ at $B_x = 0$) are fully blocked, while the light states are unblocked. On-site (i) spin- and valley-, and (ii) pure spin-mixing processes can lift the blockade close to $B = 0$ by mixing the states pointed at by the arrows. Spin- and valley-mixing processes can also lift the blockade near the crossings (gray) at $B_z \approx \Delta_{SO}/g_v\mu_B$ by mixing states from different clusters. Large enough B_x tilts the spin quantization axis from the z to x direction, mixing the blocked states with the unblocked ones, thus lifting the blockade.

by the Zeeman energy. In an out-of-plane field B_z (right), both spin and valley states are split by $g\mu_B B_z$ with their respective g_s and g_v, forming four clusters of states: one cluster of triplet states in the right dot per state in the left dot. The four fully blocked $S_z = \pm 3/2$ states are sketched in red; all other states are open and sketched in yellow.

We now examine experimentally the dependence of spin-blockade leakage current on the external magnetic field, and on the interdot tunnel coupling t. The field direction is changed by rotating the sample, and t is tuned via the middle barrier-gate voltage: More negative V_{MB} gives weather t. In Figs. 3(ai)–3(aiii) we show resulting bias triangles at zero field for various t, all weaker than in Fig. 1(a). The corresponding current measured along the detuning δ axis and its dependence on out-of-plane B_z and in-plane B_x field is mapped in Figs. 3(b) and 3(c). Line cuts are shown as a function of B_z [Fig. 3(d)] and B_x [Fig. 3(e)] around $\delta = 0$ averaged over a range of $\Delta\delta \approx 30$ μeV [≈150 μeV for Fig. 3(diii)].

Upon suppressing t, we observe in the bias triangles [Fig. 3(a)] the emergence of a resonance around $\delta = 0$ with current increasing from (i) below the noise level, to (iii) ∼1 pA. When turning on B_z [Figs. 3(b) and 3(d)], the current decreases with increasing B_z [Figs. 3(b), 3(dii), and 3(diii)] with full-width-half-maximum (FWHM) $\Delta B_z \sim 10$ mT.

This zero-field current peak could arise from mixing of the blocked and the unblocked (1,2) states by spin- or valley-mixing processes. Shown in Fig. 2, around zero field the four blocked (1,2) states can undergo either (i) simultaneous on-site spin and valley flip in the one-carrier left dot, mixing e.g., the blocked state $|\uparrow K^-\rangle_L |T_s^+ S_v\rangle_R$ with the unblocked state $|\downarrow K^+\rangle_L |T_s^+ S_v\rangle_R$, or (ii) on-site pure spin flips in the two-carrier right dot, mixing, e.g., the blocked state $|\uparrow K^-\rangle_L |T_s^+ S_v\rangle_R$ with the unblocked state $|\uparrow K^-\rangle_L |T_s^0 S_v\rangle_R$. At large enough fields such that Zeeman splittings in B_z between the mixed (1,2) states [$g_v\mu_B B_z$ for (i) and $g_s\mu_B B_z$ for (ii)] is larger than the mixing energy, the system goes into full spin blockade. The width of the zero-field current peak in B_z, therefore, contains information about the strength of the underlying mixing processes.

In most double-dot systems, this spin-mixing term is attributed to the hyperfine interaction with randomly fluctuating nuclear spin baths [14,17,19–22]. If the same applies to our system and lifts the blockade via pure spin-flip processes (ii), then the peak width $\Delta B \sim 10$ mT should correspond to the root-mean-square magnitude of the random nuclear fields B_{nuc} experienced by the localized spins. Our quantum dots ∼50 nm in radius are made of exfoliated BLG which contains only 1.01% spinful ^{13}C, yielding $B_{nuc} \sim 1$ μT using the hyperfine coupling constant $A \sim 1$ μeV calculated by Refs. [21,22] for graphene, or $B_{nuc} \sim 100$ μT using $A \sim 100$–200 μeV extracted from the leakage current peak observed in ^{13}C enriched carbon nanotubes [19]. Our observed peak width of 10 mT is, however, orders of magnitude larger, indicating that a different mechanism is responsible.

Wide zero-field peaks in Si have been attributed to finite-temperature cotunneling effects, yielding $I \propto g\mu_B B_z/\sinh(g\mu_B B_z/k_B T)$ when $t < k_B T$ [24,27,28]. For type-(ii) processes where spins are flipped in the right dot, cotunneling events have to involve virtual (1,1) states that are too high in energy to be accessible. For type-(i) processes, virtual (0,2) states are closer in energy, and cotunneling events with the lead can provide simultaneous spin and valley flips in the left dot; with $g_v = 30$ [as type-(i) processes involve valley flips] and $T \approx 100$ mK we estimate for cotunneling-induced current peaks FWHM 12 mT, similar to the measured 10 mT. In Appendix A5 [29], we measure a different device in a setup with lower electronic temperature $T \approx 45$ mK. There, we observe a narrower leakage current peak with FWHM 4–6 mT due to the lower T decreasing the width of the sinh function. The skewness of the baseline resonance of the bias triangles towards the (0,2) charge state in Fig. 3(aii) further corroborates with our conjecture, though noise and charge instability preclude definite conclusions.

Another feature observed in out-of-plane field is two side peaks occurring at $B_z \approx \pm 16.5$ mT, too narrow (FWHM ∼ 2 mT) to arise from the cotunneling effects discussed above. In the (1,2) level structure in B_z (Fig. 2), a cluster of triplet states with $|\uparrow K^+\rangle_L$ (moving up in energy) crosses the triplet with $|\uparrow K^-\rangle_L$ (moving down) at $B_z \approx \Delta_{SO}/g_v\mu_B$ (gray shading in Fig. 2). If finite mixing between

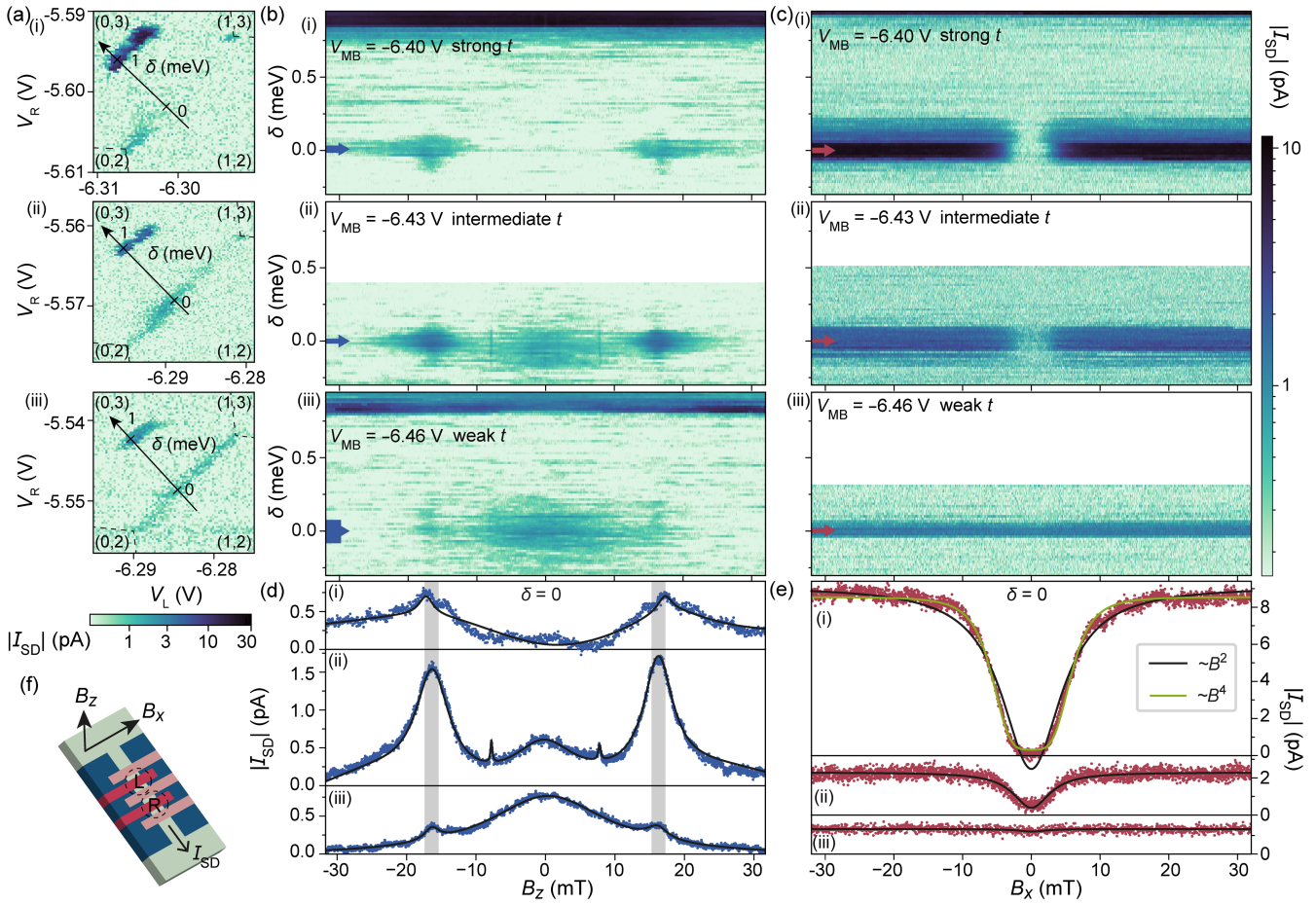

FIG. 3. (a) Bias triangles with $V_{SD} = -1$ mV for the spin-blocked transition $(1,2) \rightarrow (0,3)$ at zero magnetic field at (i) strong, (ii) intermediate, and (iii) weak interdot coupling t, at $V_{MB} = -6.40$, -6.43, and -6.46 V, respectively, with corresponding maps as functions of δ [labeled in (a)] and B-field for (b) out-of-plane field B_z, and (c) in-plane field B_x. The field orientations are indicated in (f). (d),(e): Line cuts from the respective maps averaged around zero detuning over a range $\Delta\delta$ [indicated by the width of the arrows in (b), (c), the larger range for (diii) is needed due to weak and unstable signal] with fitted curves. A B-field offset is subtracted from each map and trace, assuming for (b) and (d): the side peaks are symmetric in B_z, and for (c) and (e): the dip is centered at $B_x = 0$ T. Traces in (d) are fitted with multiple Lorentzians. In (e), empirical fits with higher order field dependence B^4 (green) describe the data better than fits of Lorentzian-shaped dips with B^2 dependence (black).

a blocked state in one triplet and an unblocked state in the other triplet exists, by a mechanism that flips valley in the left and spin in the right dot, e.g., between the blocked $|\uparrow K^+\rangle_L |T_s^+ S_v\rangle_R$ and the unblocked $|\uparrow K^-\rangle_L |T_s^0 S_v\rangle_R$, then an increase in current close to the crossing point would be expected. With $g_v \approx 30$ and side peaks at ± 16.5 mT, this implies $\Delta_{SO} \approx 30$ μeV, similar to that reported in Refs. [1,2] within a factor of 2. In a second device we observe side peaks centered at similar B_z ($\pm$16–21 mT). The higher resolution in δ there suggests that they appear at higher $\delta \approx 60$ μeV $\sim \Delta_{SO}$ instead of exactly at $\delta = 0$ (see Appendix A5 Fig. 6 [29]).

We now turn to the effect of an in-plane field B_x, perpendicular to the double-dot axis [see Fig. 3(f)]. At strong interdot coupling t [Figs. 3(ci) and 3(ei)], we observe a large leakage current at finite B_x, which is reduced at zero field. As t is weakened, the saturation leakage current decreases from 8 pA in (i) to 1.2 pA in (iii), while the width of the dip remains roughly constant.

In two-particle blockade, such a zero-field dip is usually attributed to the spin-orbit interaction [15,16,18,19,23,24]. The situation is similar here: At zero field, the Kane-Mele spin-orbit interaction dominates and all quantization axes are oriented along the z axis, splitting the (1,2) states into two clusters of six degenerate states (see Fig. 2)—the system is in spin blockade. A finite B_x lifts this blockade: not only does it lift the degeneracy, but it also tilts the quantization axis of the spin triplets towards the x axis, such that the original blocked $S_z = \pm 3/2$ states become mixed by the Zeeman field with the open states (the dark blocked states brightening in Fig. 2). Consequently, leakage current starts to increase away from $B_x = 0$. The leakage current reduces but remains finite when tilting the external magnetic field away from in plane (see Appendix. A3 [29]).

Two details of the dip deviate slightly from the standard. First, a direct mixing of blocked and unblocked states by B_x yields a regular Lorentzian line shape with a field dependence B_x^2 [15,16,18,19,24]. Here, an empirical fit with $A - C/(B_0^4 + B_x^4)$ with fitting constants A and C [Fig. 3(ei) green] shows better agreement with our data than the Lorentzian fit [Figs. 3(ei) and 3(eii), black], suggesting that state-mixing by the applied Zeeman field could be higher order. This effect is not as clearly pronounced in a second device (see Appendix A5 [29]) where measurements were taken with higher noise and fewer $B_\perp$ steps. Second, we expect the width of the dip to be strongly dependent on the interdot exchange energy caused by coupling to the (0,3) states, i.e., $\propto t^2$ [23], as it competes with the Zeeman splitting. Such a dependence is not prominent here. In a second device (Appendix A5 [29]) the dip width is larger than here by a few times, but no strong dependence on the three different t regimes was observed. These details suggest the existence of other mechanisms at play. The cotunneling process discussed earlier in the out-of-plane field cannot be responsible for the linewidth here, since $g_s \ll g_v$, it would only become relevant at much higher in-plane field.

To conclude, we examined the spin-blockade leakage current in a BLG double quantum dot at the three-carrier charge transition $(1,2) \rightarrow (0,3)$, and investigated its dependence on interdot coupling t and external magnetic field. Most of the characteristics can be understood in terms of processes similar to those observed in other quantum dot systems, but some of the details still require further investigations of the underlying mechanisms. In out-of-plane magnetic field, the dominant feature is a zero-field current peak that could arise from finite-temperature cotunneling with the leads, though explanations of the persistent side peaks have to involve other mixing mechanisms. In the in-plane magnetic field, we observe a zero-field current dip, which arises from the competition between the Zeeman effect and the Kane-Mele spin-orbit interaction; details of its line shape, however, suggest additional mechanisms are at play. We expect further studies to capture the nature of the various spin-mixing mechanisms existing in BLG in more detail, thereby paving the way for BLG spin qubits, and gaining deeper insights into the spin and valley physics.

The data supporting the findings of this study are made available via the ETH Research Collection [41].

We thank P. Märki and T. Bähler as well as the FIRST staff for their technical support. We acknowledge funding from the Core3 European Graphene Flagship Project, the Swiss National Science Foundation via NCCR Quantum Science and Technology, and the EU Spin-Nano RTN network. R. G. acknowledges funding from the European Union's Horizon 2020 research and innovation program under the Marie Skłodowska-Curie Grant Agreement No. 766025. K. W. and T. T. acknowledge support from the Elemental Strategy Initiative conducted by the MEXT, Japan, Grants No. JPMXP0112101001, No. JSPS KAKENHI Grants No. 19H05790 and No. JP20H00354.

*ctong@phys.ethz.ch

[1] A. Kurzmann, Y. Kleeorin, C. Tong, R. Garreis, A. Knothe, M. Eich, C. Mittag, C. Gold, F. K. de Vries, K. Watanabe *et al.*, Kondo effect and spin-orbit coupling in graphene quantum dots, Nat. Commun. **12**, 6004 (2021).

[2] L. Banszerus, S. Möller, C. Steiner, E. Icking, S. Trellenkamp, F. Lentz, K. Watanabe, T. Taniguchi, C. Volk, and C. Stampfer, Spin-valley coupling in single-electron bilayer graphene quantum dots, Nat. Commun. **12**, 5250 (2021).

[3] C. L. Kane and E. J. Mele, Quantum spin Hall effect in graphene, Phys. Rev. Lett. **95**, 226801 (2005).

[4] M. Eich, F. Herman, R. Pisoni, H. Overweg, A. Kurzmann, Y. Lee, P. Rickhaus, K. Watanabe, T. Taniguchi, M. Sigrist, T. Ihn, and K. Ensslin, Spin and valley states in gate-defined bilayer graphene quantum dots, Phys. Rev. X **8**, 031023 (2018).

[5] C. Tong, R. Garreis, A. Knothe, M. Eich, A. Sacchi, K. Watanabe, T. Taniguchi, V. Fal'ko, T. Ihn, K. Ensslin *et al.*, Tunable valley splitting and bipolar operation in graphene quantum dots, Nano Lett. **21**, 1068 (2021).

[6] R. Garreis, A. Knothe, C. Tong, M. Eich, C. Gold, K. Watanabe, T. Taniguchi, V. Fal'ko, T. Ihn, K. Ensslin, and A. Kurzmann, Shell filling and trigonal warping in graphene quantum dots, Phys. Rev. Lett. **126**, 147703 (2021).

[7] A. Kurzmann, M. Eich, H. Overweg, M. Mangold, F. Herman, P. Rickhaus, R. Pisoni, Y. Lee, R. Garreis, C. Tong, K. Watanabe, T. Taniguchi, K. Ensslin, and T. Ihn, Excited states in bilayer graphene quantum dots, Phys. Rev. Lett. **123**, 026803 (2019).

[8] L. Banszerus, A. Rothstein, T. Fabian, S. Möller, E. Icking, S. Trellenkamp, F. Lentz, D. Neumaier, K. Watanabe, T. Taniguchi *et al.*, Electron–hole crossover in gate-controlled bilayer graphene quantum dots, Nano Lett. **20**, 7709 (2020).

[9] S. Möller, L. Banszerus, A. Knothe, C. Steiner, E. Icking, S. Trellenkamp, F. Lentz, K. Watanabe, T. Taniguchi, L. I. Glazman, V. I. Fal'ko, C. Volk, and C. Stampfer, Probing two-electron multiplets in bilayer graphene quantum dots, Phys. Rev. Lett. **127**, 256802 (2021).

[10] C. Tong, A. Kurzmann, R. Garreis, W. W. Huang, S. Jele, M. Eich, L. Ginzburg, C. Mittag, K. Watanabe, T. Taniguchi *et al.*, Pauli blockade of tunable two-electron spin and valley states in graphene quantum dots, Phys. Rev. Lett. **128**, 067702 (2022).

[11] L. M. Gächter, R. Garreis, J. D. Gerber, M. J. Ruckriegel, C. Tong, B. Kratochwil, F. K. de Vries, A. Kurzmann, K. Watanabe, T. Taniguchi *et al.*, Single-shot spin readout in graphene quantum dots, PRX Quantum **3**, 020343 (2022).

[12] R. Garreis, J. D. Gerber, V. Stará, C. Tong, C. Gold, M. Röösli, K. Watanabe, T. Taniguchi, K. Ensslin, T. Ihn, and A. Kurzmann, Counting statistics of single electron

transport in bilayer graphene quantum dots, Phys. Rev. Res. **5**, 013042 (2023).
[13] L. Banszerus, K. Hecker, S. Möller, E. Icking, K. Watanabe, T. Taniguchi, C. Volk, and C. Stampfer, Spin relaxation in a single-electron graphene quantum dot, Nat. Commun. **13**, 3637 (2022).
[14] F. H. Koppens, J. A. Folk, J. M. Elzerman, R. Hanson, L. W. Van Beveren, I. T. Vink, H.-P. Tranitz, W. Wegscheider, L. P. Kouwenhoven, and L. M. Vandersypen, Control and detection of singlet-triplet mixing in a random nuclear field, Science **309**, 1346 (2005).
[15] A. Pfund, I. Shorubalko, K. Ensslin, and R. Leturcq, Suppression of spin relaxation in an InAs nanowire double quantum dot, Phys. Rev. Lett. **99**, 036801 (2007).
[16] S. Nadj-Perge, S. M. Frolov, J. W. W. van Tilburg, J. Danon, Y. V. Nazarov, R. Algra, E. P. A. M. Bakkers, and L. P. Kouwenhoven, Disentangling the effects of spin-orbit and hyperfine interactions on spin blockade, Phys. Rev. B **81**, 201305(R) (2010).
[17] C. Mittag, J. V. Koski, M. Karalic, C. Thomas, A. Tuaz, A. T. Hatke, G. C. Gardner, M. J. Manfra, J. Danon, T. Ihn *et al.*, Few-electron single and double quantum dots in an InAs two-dimensional electron gas, PRX Quantum **2**, 010321 (2021).
[18] R. Li, F. E. Hudson, A. S. Dzurak, and A. R. Hamilton, Pauli spin blockade of heavy holes in a silicon double quantum dot, Nano Lett. **15**, 7314 (2015).
[19] H. O. H. Churchill, A. J. Bestwick, J. W. Harlow, F. Kuemmeth, D. Marcos, C. H. Stwertka, S. K. Watson, and C. M. Marcus, Electron–nuclear interaction in 13c nanotube double quantum dots, Nat. Phys. **5**, 321 (2009).
[20] O. N. Jouravlev and Y. V. Nazarov, Electron transport in a double quantum dot governed by a nuclear magnetic field, Phys. Rev. Lett. **96**, 176804 (2006).
[21] O. V. Yazyev, Hyperfine interactions in graphene and related carbon nanostructures, Nano Lett. **8**, 1011 (2008).
[22] J. Fischer, B. Trauzettel, and D. Loss, Hyperfine interaction and electron-spin decoherence in graphene and carbon nanotube quantum dots, Phys. Rev. B **80**, 155401 (2009).
[23] J. Danon and Y. V. Nazarov, Pauli spin blockade in the presence of strong spin-orbit coupling, Phys. Rev. B **80**, 041301(R) (2009).
[24] G. Yamahata, T. Kodera, H. O. H. Churchill, K. Uchida, C. M. Marcus, and S. Oda, Magnetic field dependence of pauli spin blockade: A window into the sources of spin relaxation in silicon quantum dots, Phys. Rev. B **86**, 115322 (2012).
[25] A. Knothe and V. Fal'ko, Quartet states in two-electron quantum dots in bilayer graphene, Phys. Rev. B **101**, 235423 (2020).
[26] A. Knothe, L. I. Glazman, and V. I. Fal'ko, Tunneling theory for a bilayer graphene quantum dot's single-and two-electron states, New J. Phys. **24**, 043003 (2022).
[27] N. Lai, W. Lim, C. Yang, F. Zwanenburg, W. Coish, F. Qassemi, A. Morello, and A. Dzurak, Pauli spin blockade in a highly tunable silicon double quantum dot, Sci. Rep. **1**, 110 (2011).
[28] F. Qassemi, W. A. Coish, and F. K. Wilhelm, Stationary and transient leakage current in the pauli spin blockade, Phys. Rev. Lett. **102**, 176806 (2009).
[29] See Supplemental Material at http://link.aps.org/supplemental/10.1103/PhysRevLett.133.017001 for discussions on the sample and fabrication methods, a more detailed discussion on the (1,2) and (0,3) states, an in-between in-plane and out-of-plane magnetic field measurement, report on leakage current observed at (1,1) and (0,2) transitions from the valley blockade effect, and data taken from a different device for comparison and relevant discussions, which includes Refs. [12,30–40].
[30] H. Overweg, H. Eggimann, X. Chen, S. Slizovskiy, M. Eich, R. Pisoni, Y. Lee, P. Rickhaus, K. Watanabe, T. Taniguchi *et al.*, Electrostatically induced quantum point contacts in bilayer graphene, Nano Lett. **18**, 553 (2018).
[31] L. Wang, I. Meric, P. Huang, Q. Gao, Y. Gao, H. Tran, T. Taniguchi, K. Watanabe, L. Campos, D. Muller *et al.*, One-dimensional electrical contact to a two-dimensional material, Science **342**, 614 (2013).
[32] T. Ohta, A. Bostwick, T. Seyller, K. Horn, and E. Rotenberg, Controlling the electronic structure of bilayer graphene, Science **313**, 951 (2006).
[33] E. McCann, Asymmetry gap in the electronic band structure of bilayer graphene, Phys. Rev. B **74**, 161403(R) (2006).
[34] J. B. Oostinga, H. B. Heersche, X. Liu, A. F. Morpurgo, and L. M. Vandersypen, Gate-induced insulating state in bilayer graphene devices, Nat. Mater. **7**, 151 (2008).
[35] A. L. Buchachenko and V. L. Berdinsky, Electron spin catalysis, Chem. Rev. **102**, 603 (2002).
[36] E. A. Laird, J. M. Taylor, D. P. DiVincenzo, C. M. Marcus, M. P. Hanson, and A. C. Gossard, Coherent spin manipulation in an exchange-only qubit, Phys. Rev. B **82**, 075403 (2010).
[37] R. Garreis, C. Tong, J. Terle, M. J. Ruckriegel, J. D. Gerber, L. M. Gächter, K. Watanabe, T. Taniguchi, T. Ihn, K. Ensslin *et al.*, Long-lived valley states in bilayer graphene quantum dots, Nat. Phys. 1 (2024).
[38] D. Weinmann, W. Häusler, and B. Kramer, Spin blockades in linear and nonlinear transport through quantum dots, Phys. Rev. Lett. **74**, 984 (1995).
[39] T. Hatano, Y. Tokura, S. Amaha, T. Kubo, S. Teraoka, and S. Tarucha, Excitation spectroscopy of few-electron states in artificial diatomic molecules, Phys. Rev. B **87**, 241414(R) (2013).
[40] S. Amaha, W. Izumida, T. Hatano, S. Tarucha, K. Kono, and K. Ono, Spin blockade in a double quantum dot containing three electrons, Phys. Rev. B **89**, 085302 (2014).
[41] C. Tong, F. Ginzel, A. Kurzmann, R. Garreis, L. Ostertag, J. D. Gerber, W. W. Huang, K. Watanabe, T. Taniguchi, G. Burkard, J. Danon, T. Ihn, and K. Ensslin, Data repository: Three-carrier spin blockade and coupling in bilayer graphene double quantum dots (2024), 20.500.11850/668625.